© 2016. Published by The Company of Biologists Ltd | Journal of Cell Science (2016) 129, 2757-2766 doi:10.1242/jcs.185983

RESEARCH ARTICLE

Ttll9$^{-/-}$ mice sperm flagella show shortening of doublet 7, reduction of doublet 5 polyglutamylation and a stall in beating

Alu Konno[1,2], Koji Ikegami[1,3], Yoshiyuki Konishi[1], Hyun-Jeong Yang[1], Manabu Abe[4], Maya Yamazaki[4], Kenji Sakimura[4], Ikuko Yao[2,3], Kogiku Shiba[5], Kazuo Inaba[5] and Mitsutoshi Setou[1,2,3,6,7,8,*]

ABSTRACT

Nine outer doublet microtubules in axonemes of flagella and cilia are heterogeneous in structure and biochemical properties. In mammalian sperm flagella, one of the factors to generate the heterogeneity is tubulin polyglutamylation, although the importance of the heterogeneous modification is unclear. Here, we show that a tubulin polyglutamylase *Ttll9* deficiency (*Ttll9*$^{-/-}$) causes a unique set of phenotypes related to doublet heterogeneity. *Ttll9*$^{-/-}$ sperm axonemes had frequent loss of a doublet and reduced polyglutamylation. Intriguingly, the doublet loss selectively occurred at the distal region of doublet 7, and reduced polyglutamylation was observed preferentially on doublet 5. *Ttll9*$^{-/-}$ spermatozoa showed aberrant flagellar beating, characterized by frequent stalls after anti-hook bending. This abnormal motility could be attributed to the reduction of polyglutamylation on doublet 5, which probably occurred at a position involved in the switching of bending. These results indicate that mammalian *Ttll9* plays essential roles in maintaining the normal structure and beating pattern of sperm flagella by establishing normal heterogeneous polyglutamylation patterns.

KEY WORDS: Axoneme, Flagella, Polyglutamylation, Sperm, Tubulin

INTRODUCTION

Eukaryotic flagella and cilia are microtubule (MT)-based organelles that have a common structure called the axoneme. Motile axonemes are complex molecular machineries composed of dyneins and regulatory components attached to scaffolding MTs (Inaba, 2007, 2011). Axonemal MTs are arranged in so-called 9+2 structures, comprising nine outer doublet MTs and two central singlet MTs. Although the outer doublets are often referred to as rotationally symmetrical, several structural heterogeneities are also reported (Heuser et al., 2012).

One of the tubulin post-translational modifications (PTMs), polyglutamylation, shows an interdoublet heterogeneity, where doublets 1, 5, 6 and 9 have higher levels of modification than other doublets in mammalian sperm flagella (Fouquet et al., 1996; Prigent et al., 1996; Kann et al., 2003). Polyglutamylation is a unique PTM by which variable lengths of glutamate side-chains are attached to the C-terminal tail (CTT) of α- and β-tubulins (Eddé et al., 1990). Because tubulin PTMs can affect the structural and chemical properties of MTs (Wloga and Gaertig, 2010; Konno et al., 2012; Magiera and Janke, 2014), establishing proper polyglutamylation patterns is essential for correct sperm flagellar structures and/or functions. However, mechanisms for establishing the heterogeneous polyglutamylation pattern and the importance of the interdoublet heterogeneity are almost completely unknown.

Polyglutamylation is catalyzed by a subset of tubulin tyrosine ligase-like proteins (TTLLs) (Janke et al., 2005; Ikegami et al., 2006; van Dijk et al., 2007). The importance of the PTMs of motile flagella and cilia has been reported previously in various models, such as mouse (Ikegami et al., 2010; Lee et al., 2013), ependymal cells (Bosch Grau et al., 2013), *Tetrahymena* (Wloga et al., 2010; Suryavanshi et al., 2010) and *Chlamydomonas* (Kubo et al., 2010, 2012). Recently, a few reports on transgenic mouse models have also underlined the importance of polyglutamylation in spermatozoa. For example, severely shortened flagella have been found in *Ttll1*-knockout mice (Ikegami et al., 2010), and subfertility has been reported in *Stamp*$^{tm/tm}$ mice, which have a truncation in the non-catalytic region of *Ttll5*, due to structural defects of sperm flagella and reduced motility (Lee et al., 2013).

Here, we have investigated the sperm structure and motility of transgenic mice lacking polyglutamylase *Ttll9* (*Ttll9*$^{-/-}$). *Ttll9*$^{-/-}$ causes infertility in male mice owing to reduced sperm count and defective sperm motility. We demonstrate that *Ttll9*$^{-/-}$ sperm axonemes lose doublet 7 at distal principal pieces and show reduced tubulin polyglutamylation, with a reduction in polyglutamylation of doublet 5 being the most remarkable. We also show that reduced motility of *Ttll9*$^{-/-}$ spermatozoa is caused by frequent stalls of flagella, which is indicative of defective switching in the bending direction. This tendency of the stall patterns seems to be caused, at least partly, by the reduction of polyglutamylation on doublet 5, probably at a position involved in the switching between bending directions. These results indicate that the establishment of heterogeneous polyglutamylation by *Ttll9* is essential for both normal structure and beating pattern of murine sperm flagella.

RESULTS

Infertility of *Ttll9*$^{-/-}$ male mice

We examined the expression pattern of *Ttll9* with reverse-transcriptase (RT)-PCR and found strong expression in testes of wild-type mice (Fig. 1A). The *Ttll9* transcript was not detected in brain, probably owing to limited expression in that tissue (Bosch Grau et al., 2013; Zeisel et al., 2015). To identify the area of expression of *Ttll9* in wild-type testes, we performed *in situ*

[1]Department of Cellular and Molecular Anatomy, Hamamatsu University School of Medicine, Hamamatsu, Shizuoka 4313192, Japan. [2]Preeminent Medical Photonics Education & Research Center, Hamamatsu University School of Medicine, Hamamatsu, Shizuoka 4313192, Japan. [3]International Mass Imaging Center, Hamamatsu University School of Medicine, Hamamatsu, Shizuoka 4313192, Japan. [4]Department of Cellular Neurobiology, Brain Research Institute, Niigata University, Niigata 9518585, Japan. [5]Shimoda Marine Research Center, University of Tsukuba, Shimoda, Shizuoka 4150025, Japan. [6]Department of Anatomy, The University of Hong Kong, 6/F, William MW Mong Block, 21 Sassoon Road, Pokfulam, Hong Kong SAR, China. [7]Division of Neural Systematics, National Institute for Physiological Sciences, National Institutes of Natural Sciences, Okazaki, Aichi 4440867, Japan. [8]Riken Center for Molecular Imaging Science, Kobe, Hyogo 6500047, Japan.

*Author for correspondence (setou@hama-med.ac.jp)

M.S., 0000-0002-1302-6467

Received 19 January 2016; Accepted 31 May 2016

Journal of Cell Science (2016) 129, 2757-2766 doi:10.1242/jcs.185983

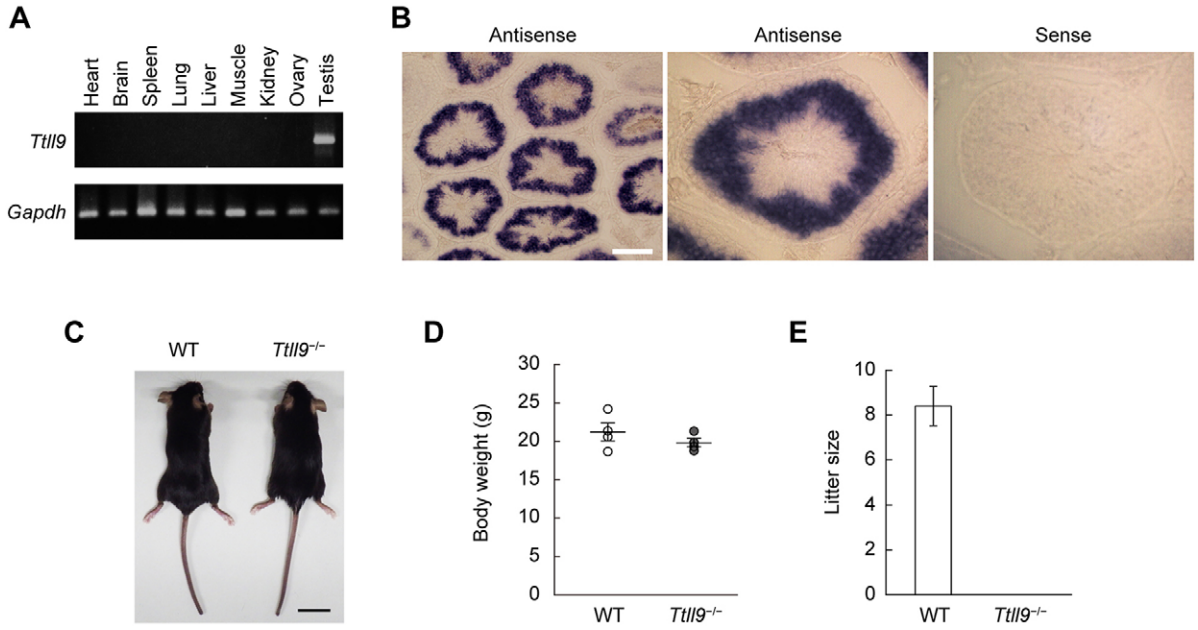

Fig. 1. Infertility in *Ttll9*$^{-/-}$ male mice. (A) RT-PCR analysis of the *Ttll9* transcript. (B) *In situ* hybridization of *Ttll9* transcripts on testicular cross sections. Scale bar: 100 µm. (C) Gross morphology of wild-type (WT) and *Ttll9*$^{-/-}$ male mice at 8 weeks of age. Scale bar: 2 cm. (D) Body weight of WT and *Ttll9*$^{-/-}$ male mice at 8 weeks of age (n=4). P=0.32 (Student's t-test, two-tailed). Data are plots of raw values for each sample (circles) and mean±s.e.m. (E) *In vivo* fertilization assay. n=5 (WT) and n=4 (*Ttll9*$^{-/-}$). P<0.001 (Welch's t-test, two-tailed). Data are mean±s.e.m. n values are the number of mice analyzed.

hybridization on cross sections (Fig. 1B). *Ttll9* expression was detected inside of seminiferous tubules with a lack of signal at the most peripheral regions, similar to that of many genes involved in spermatogenesis and/or sperm function.

To understand the importance of polyglutamylation in mammalian sperm function, we generated tubulin polyglutamylase *Ttll9*-deficient (*Ttll9*$^{-/-}$) mice, where a stop codon introduced by a frameshift resulted in premature termination of translation (Fig. S1A–D). The *Ttll9*$^{-/-}$ mice did not show a coughing-like phenotype or hydrocephalus, indicating no deficiency in respiratory and ependymal cilia. They also showed neither apparent polydactylism nor polycystic kidneys. Although the external morphology of *Ttll9*$^{-/-}$ mice seemed normal (Fig. 1C), and their body weight was comparable to that of wild-type mice (Fig. 1D), *Ttll9*$^{-/-}$ males failed to sire pups (Fig. 1E), despite normal mating behavior and ability to deposit a plug.

Reduced sperm count and sperm polyglutamylation levels in *Ttll9*$^{-/-}$ males

To reveal the cause of male infertility, we observed the testes of *Ttll9*$^{-/-}$ males. Visual inspection of the testicular phenotype of *Ttll9*$^{-/-}$ males revealed that the external morphology and the size of wild-type and *Ttll9*$^{-/-}$ testes were comparable (Fig. 2A,B). Cross sections of *Ttll9*$^{-/-}$ testes also showed no apparent histochemical defects in their gross structures (Fig. 2C). These observations indicate that the morphogenesis of testes and early spermatogenesis are not severely affected in *Ttll9*$^{-/-}$ mice. To evaluate the effect of *Ttll9* knockout on polyglutamylation, we performed immunoblotting with antibodies against polyglutamate side-chain (polyE) and α-tubulin (12G10) (Fig. 1D,E). The blots showed a reduction of tubulin polyglutamylation in *Ttll9*$^{-/-}$ testes.

We then analyzed epididymal spermatozoa and found that the sperm count in *Ttll9*$^{-/-}$ cauda epididymides was significantly decreased (Fig. 2F). The polyglutamylation level of *Ttll9*$^{-/-}$ spermatozoa was also reduced (Fig. 2G,H). Tubulins seem to be the only major group of proteins to be abundantly polyglutamylated in murine spermatozoa (Fig. S1E). By using light microscopy, we observed that the head and tail of *Ttll9*$^{-/-}$ spermatozoa were often detached (Fig. 2I). Nevertheless, some spermatozoa showed a normal appearance with a hook-shaped head and elongated flagellum.

Ttll9$^{-/-}$ sperm axonemes show a frequently shortened doublet 7 and a reduction of polyglutamylation preferentially on doublet 5

To examine the ultrastructure of *Ttll9*$^{-/-}$ spermatozoa, we performed transmission electron microscopy (TEM) analysis. TEM analysis showed that the lumens of seminiferous tubules (Fig. 3A) and cauda epididymides (Fig. 3B) of *Ttll9*$^{-/-}$ males contained fewer spermatozoa than did wild-type males. Cell debris was often observed in the lumen of *Ttll9*$^{-/-}$ epididymides, but most *Ttll9*$^{-/-}$ flagella in cauda epididymides showed normal axonemal structures at midpieces (Fig. 3C). At distal principal pieces, however, the frequent loss of a single doublet, doublet 7, was observed (Fig. 3C, arrow). This demonstrates that doublet 7 was shortened in *Ttll9*$^{-/-}$ sperm flagella. In some cases, an electron-dense mass was found in the place where doublet 7 was originally present (Fig. S2A, arrow). Occasionally, a possible breakage of a doublet was observed in longitudinal sections (Fig. S2B). The shortening of the doublet 7 was never observed in *Ttll9*$^{-/-}$ testes (Fig. 3A). Minor abnormalities included ectopic and/or excess doublet(s) or outer dense fibers (ODFs) and a distorted fibrous sheath (Fig. S2C). The ultrastructure of respiratory cilia was normal in *Ttll9*$^{-/-}$ tracheae (Fig. S2D). The amount of VDAC3 was not altered in *Ttll9*$^{-/-}$ spermatozoa (Fig. S2E), although VDAC3 deficiency is reported to result in the doublet 7 loss (Sampson et al., 2001).

We further analyzed the position where the doublet 7 loss occurs along the flagellum. In mouse spermatozoa, nine ODFs at a proximal flagellum tapered and decreased in number with fixed

Journal of Cell Science (2016) 129, 2757-2766 doi:10.1242/jcs.185983

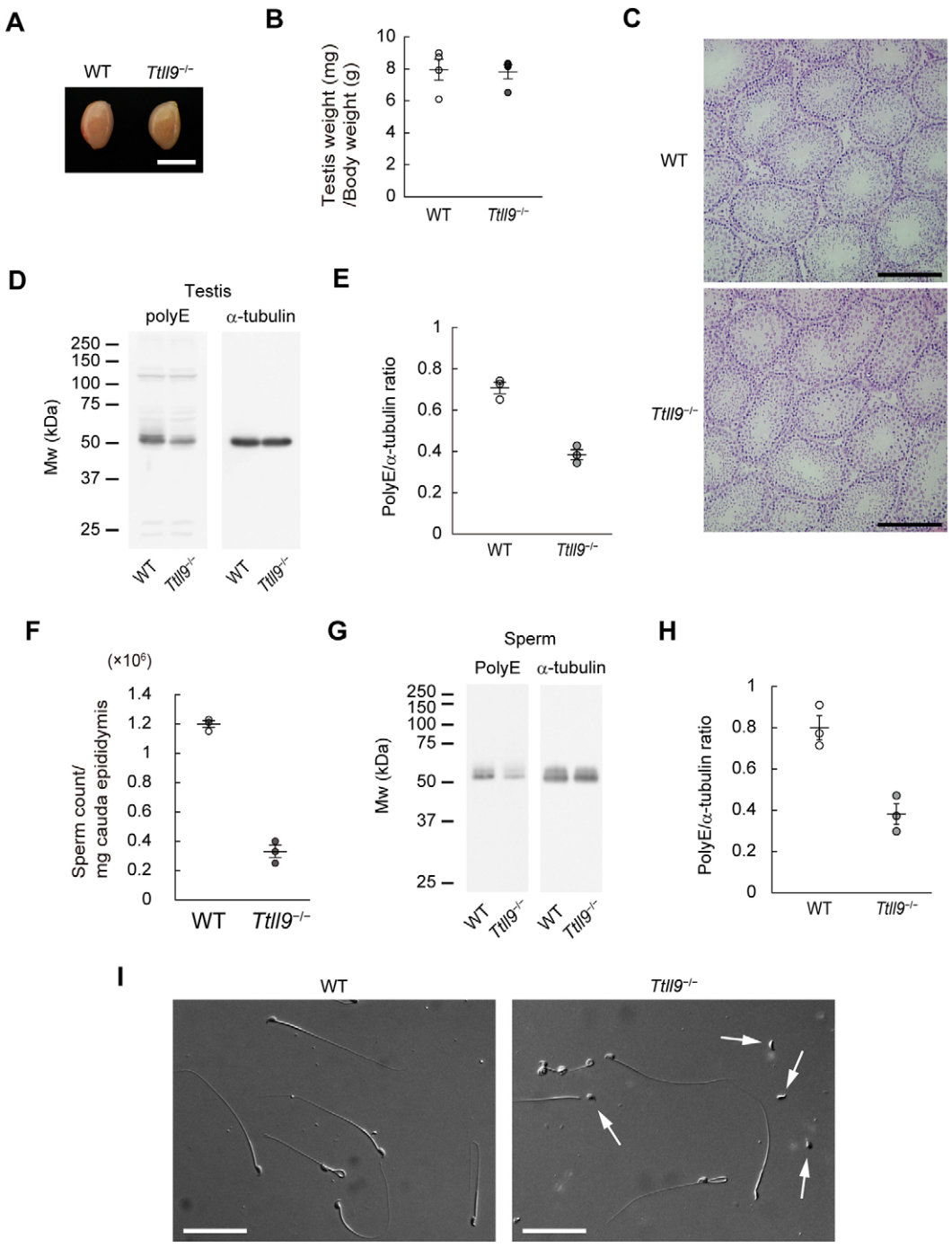

Fig. 2. Reduced polyglutamylation in *Ttll9*$^{-/-}$ testes and spermatozoa. (A) Morphology of testes. Scale bar: 5 mm. WT, wild-type. (B) Normalized testicular weight (n=4 mice per genotype). P=0.88 (Student's t-test, two-tailed). Data are plots of values for each sample (circles) and mean±s.e.m. (C) Hematoxylin and eosin staining of testes. Scale bars: 200 µm. (D) Western blot of total testis proteins (representative image) and (E) quantification (n=3 mice per genotype). P<0.001 (Student's t-test). Data are plots of values for each sample (circles) and mean±s.e.m. (F) Normalized epididymal sperm count (n=3 mice per genotype). P<0.001 (Student's t-test, two-tailed). Data are plots of values for each sample (circles) and mean±s.e.m. (G) Western blot of total sperm proteins (representative image) and (H) quantification (n=3 mice per genotype). P=0.006 (Student's t-test, two-tailed). Data are plots of values for each sample (circles) and mean±s.e.m. (I) Morphology of epididymal spermatozoa. Arrows indicate detachment of the head from the tail. Scale bars: 50 µm.

order toward the endpiece, where no ODFs remained (Fig. 3D). We noticed that the loss of doublet 7 always occurred posterior to the point of ODF 7 termination (Fig. 3D,E). At the most distal region where no ODF was present, doublet 7 was missing in more than half of the *Ttll9*$^{-/-}$ axonemes (Fig. 3E).

Outer doublet MTs in murine sperm axonemes are heterogeneous in polyglutamylation – the PTM level of doublets 1, 5, 6 and 9 is higher than that of the others (Fouquet et al., 1996). We conducted immunogold electron microscopy analysis to assess the effect of *Ttll9* loss on the heterogeneous modification pattern (Fig. 3F; Fig. S2F,G). Cross sections of proximal midpieces, where most *Ttll9*$^{-/-}$ axonemes have normal structure, were analyzed. Using an antibody against α-tubulin (DM1A), we found that the mean particle numbers on each axoneme were comparable in wild-type

Journal of Cell Science (2016) 129, 2757-2766 doi:10.1242/jcs.185983

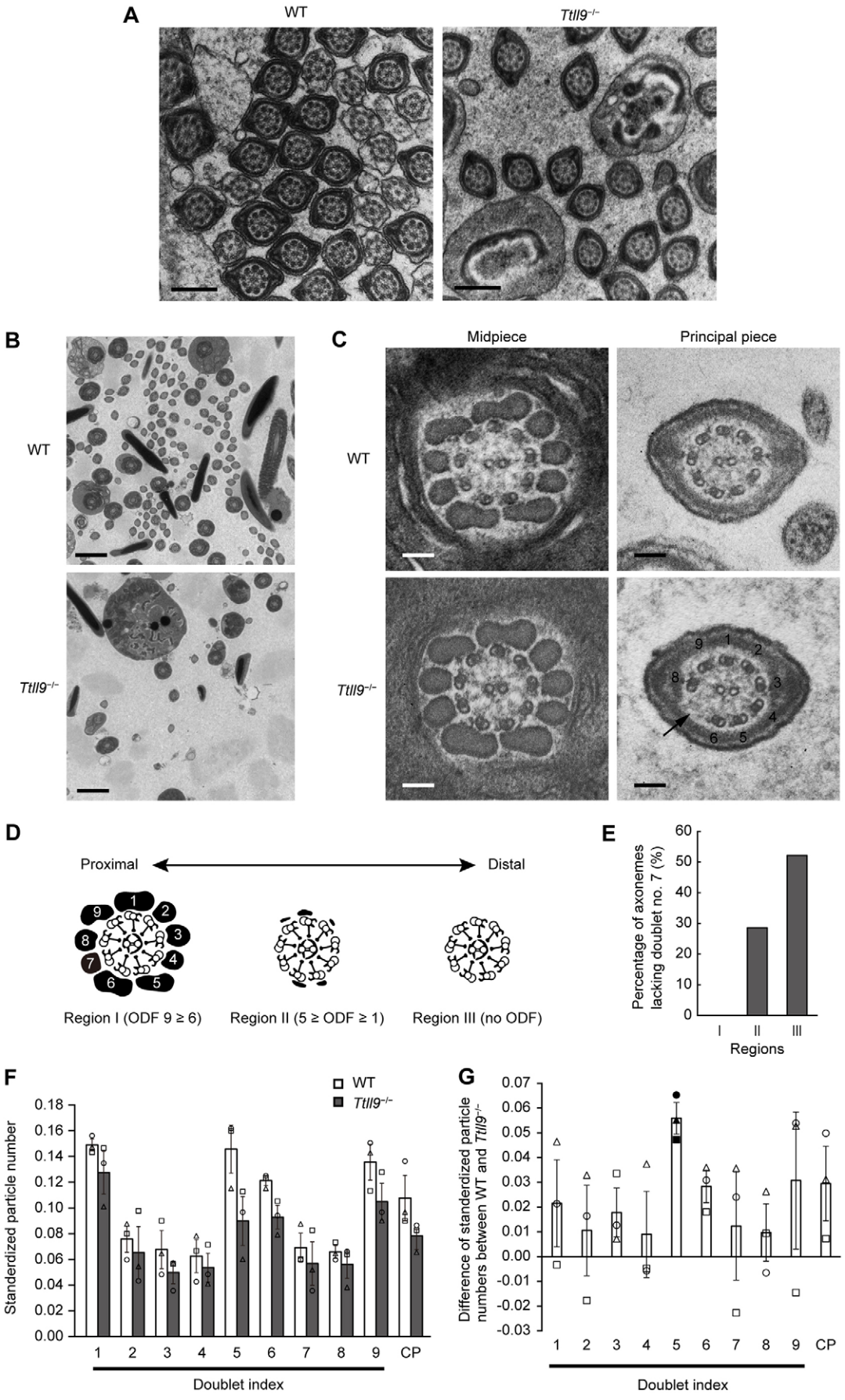

Fig. 3. See next page for legend.

Journal of Cell Science (2016) 129, 2757-2766 doi:10.1242/jcs.185983

Fig. 3. TEM analysis of spermatozoa. (A,B) Electron micrographs of spermatozoa in testes (A) and in cauda epididymides (B) of wild-type (WT) and *Ttll9*$^{-/-}$ mice. Scale bars: 500 nm (A); 2 µm (B). (C) Cross sections of WT and *Ttll9*$^{-/-}$ sperm flagella. The arrow indicates the loss of doublet 7 in *Ttll9*$^{-/-}$ flagella. Scale bars: 100 nm. (D) The order of ODF loss along a flagellum. Region I, proximal part with all ODFs; region II, middle part where ODF 7 was lost; region III, distal part with no ODFs. (E) Percentage of flagella with doublet 7 loss in each region defined in D. *n*=121 flagella cross sections. (F) Standardized particle number and particle distribution per section with polyE antibody. The number of gold particles attached on each doublet or on a pair of central singlet MTs per single axonemal ultrathin section at midpieces. *n*=862 particles from 205 sections (WT) and 776 particles from 235 sections (*Ttll9*$^{-/-}$). Circles, triangles and squares represent the independent experimental sets. Data are mean±s.e.m. The distribution of gold particles was uneven [$P<0.001$ (WT and *Ttll9*$^{-/-}$), chi-square test]. CP, central pair. (G) Differences in standardized particle numbers between WT and *Ttll9*$^{-/-}$ flagella. Circles, triangles and squares represent independent experimental sets. Black-filled marks indicate the doublet showing the largest reduction in each experimental set. Note that the doublet 5 consistently showed the largest reduction in polyglutamylation-labeling gold particles in all independent experiments. Data are mean±s.e.m. Doublet 5 is the outlier ($P<0.05$, Grubbs' test, one-tailed).

and *Ttll9*$^{-/-}$ flagella (Fig. S2H). The particle numbers on each MT set were almost uniform, although appearing to be slightly decreased on doublet 7 in *Ttll9*$^{-/-}$ sperm flagella compared to wild-type samples (Fig. S2J).

Using the polyE antibody, we found that the reduction of particle numbers in *Ttll9*$^{-/-}$ axonemes was not significant but did show a trend towards decreasing (Fig. S2I), probably because we investigated axonemes with normal ultrastructures, which are expected to have a less severe reduction of the PTM. Among ten MT sets (nine outer doublets and the central pair), doublet 5 showed the largest reduction in the amount of polyglutamylation (Fig. 3F). The largest reduction of particle number on doublet 5 was reproducibly detected in three independent experiments, whereas other doublets showed large variances (Fig. 3G). Statistical analysis revealed that the reduction in particle number on doublet 5 was a significant outlier ($P<0.05$, Grubbs' test, one tailed).

Ttll9$^{-/-}$ sperm flagella show defective motility

We performed motility analysis to evaluate the effect of *Ttll9* knockout on sperm flagellar motility with high-speed charge-coupled device (CCD) camera recordings. Trajectories of *Ttll9*$^{-/-}$ spermatozoa showed reduced percent motility (percentage of motile spermatozoa) and progressive motility compared with those of wild-type spermatozoa (Fig. 4A–C; Movie 1). We then focused on the flagellar waveforms of motile *Ttll9*$^{-/-}$ spermatozoa. At higher magnification, wild-type flagella showed smooth wave propagation, whereas *Ttll9*$^{-/-}$ flagella exhibited irregular beats with intervening stalls that continued for a variable time period (Movie 2).

Because murine spermatozoa have a hook-shaped head, the direction of flagellar bending can be defined as pro-hook and anti-hook bends (Ishijima et al., 2002). To relate the axonemal geometry with beating direction, we performed TEM analysis. The head of the murine spermatozoa protrudes posteriorly at the anti-hook side, and one can observe the protrusion and the cross section of the proximal flagellum at the same time in a single spermatozoa. TEM analysis revealed that doublet 1 is at the pro-hook side and doublets 5 and 6 are at the anti-hook side in murine spermatozoa (Fig. S2K). We conducted curvature analysis with flagellar waveform traces to assess the characteristics of the stall, and the relationship between the stall and the axonemal architecture (Fig. 4D; Fig. S3). Beat patterns were classified into four categories – normal, stalls after pro- and anti-hook bend (pro-hook stall and anti-hook stall, respectively), and double stall with pro- and anti-hook stall at the same time in a single flagellum. Fig. 4D shows superpositions of representative waveforms (top) and corresponding curvature plots (bottom) of the four types of beat patterns. Two thirds of the *Ttll9*$^{-/-}$ flagella showed one of the three stall patterns and, among them, anti-hook stall was the most frequent (Fig. 4E).

DISCUSSION

In the present study, we reveal that the loss of *Ttll9* causes a unique set of abnormalities related to the heterogeneity of axonemal structures and polyglutamylation in murine sperm flagella – i.e. the shortening of doublet 7 and the reduction of the level of polyglutamylation preferentially on doublet 5. Our data suggest that the abnormal motility of *Ttll9*$^{-/-}$ spermatozoa seems to be explained by the reduction of polyglutamylation on doublet 5.

The selective shortening of doublet 7 is a unique phenotype of *Ttll9*$^{-/-}$ sperm flagella. This was never observed in *Ttll9*$^{-/-}$ testes (Fig. 3A), indicating that the cause of the shortening is not defects in axoneme assembly. A possible cause of the specific shortening of the doublet 7 is severing of the doublet. Indeed, we observed evidence for possible severing of a doublet (Fig. S2B). The extra doublet observed can sometimes emerge when severed doublet 7 is dislocated proximally. Another cause is the depolymerization or degradation of MTs. An amorphous electron-dense mass found in the place of doublet 7 could be the remnant of the depolymerized or degraded doublet. Thus, these mechanisms – severing and depolymerization and/or degradation – could underlie the shortening of doublet 7 in *Ttll9*$^{-/-}$ sperm flagella. Severing and depolymerization seems to be prevented by mechanical support from the associated ODF 7 in *Ttll9*$^{-/-}$ spermatozoa, because the loss of doublet 7 always occurred distal to the level of the ODF 7 termination.

Destabilization of axonemal MTs caused by loss of a polyglutamylase has been reported in other models (Pathak et al., 2011; Lee et al., 2012). In contrast, Kubo et al. (2015) have reported that reduced polyglutamylation through the loss of the TTLL9–FAP234 complex stabilizes *Chlamydomonas* flagella by affecting the turnover rate of tubulin at the tips. The inconsistency might be explained by the fact that sperm flagella do not have the cytoplasmic pool of tubulin required for turnover, and their stability is likely to be determined by different mechanisms from those of *Chlamydomonas*. The selective loss of doublet 7 implies that the role of polyglutamylation in sperm flagella is complex and that outer doublet MTs are more heterogeneous than generally considered. Because doublet 7 is one of the MT subsets that have lower polyglutamylation in mammalian spermatozoa, even mild reduction of the PTM might have a larger effect. Nonetheless, we did not observe the loss of the other axonemal MTs with lower polyglutamylation levels (i.e. doublets 2, 3, 4 and 8), indicating the involvement of other factors.

Interestingly, the loss of doublet 7 has been reported previously for spermatozoa of VDAC3-deficient mice (Sampson et al., 2001). VDAC3 is a mitochondrial outer membrane protein but is also a component of ODFs in bovine spermatozoa (Hinsch et al., 2004), and some other VDACs are also thought to be present in mammalian sperm flagella (Liu et al., 2009). VDAC3 does not have glutamate-rich regions, which can be targets for polyglutamylation (van Dijk et al., 2008). Thus, it might not be possible that VDAC3 is polyglutamylated by TTLL9 and that the phenocopy is caused by the loss of polyglutamylation on VDAC3. Indeed, tubulins are the only

Journal of Cell Science (2016) 129, 2757-2766 doi:10.1242/jcs.185983

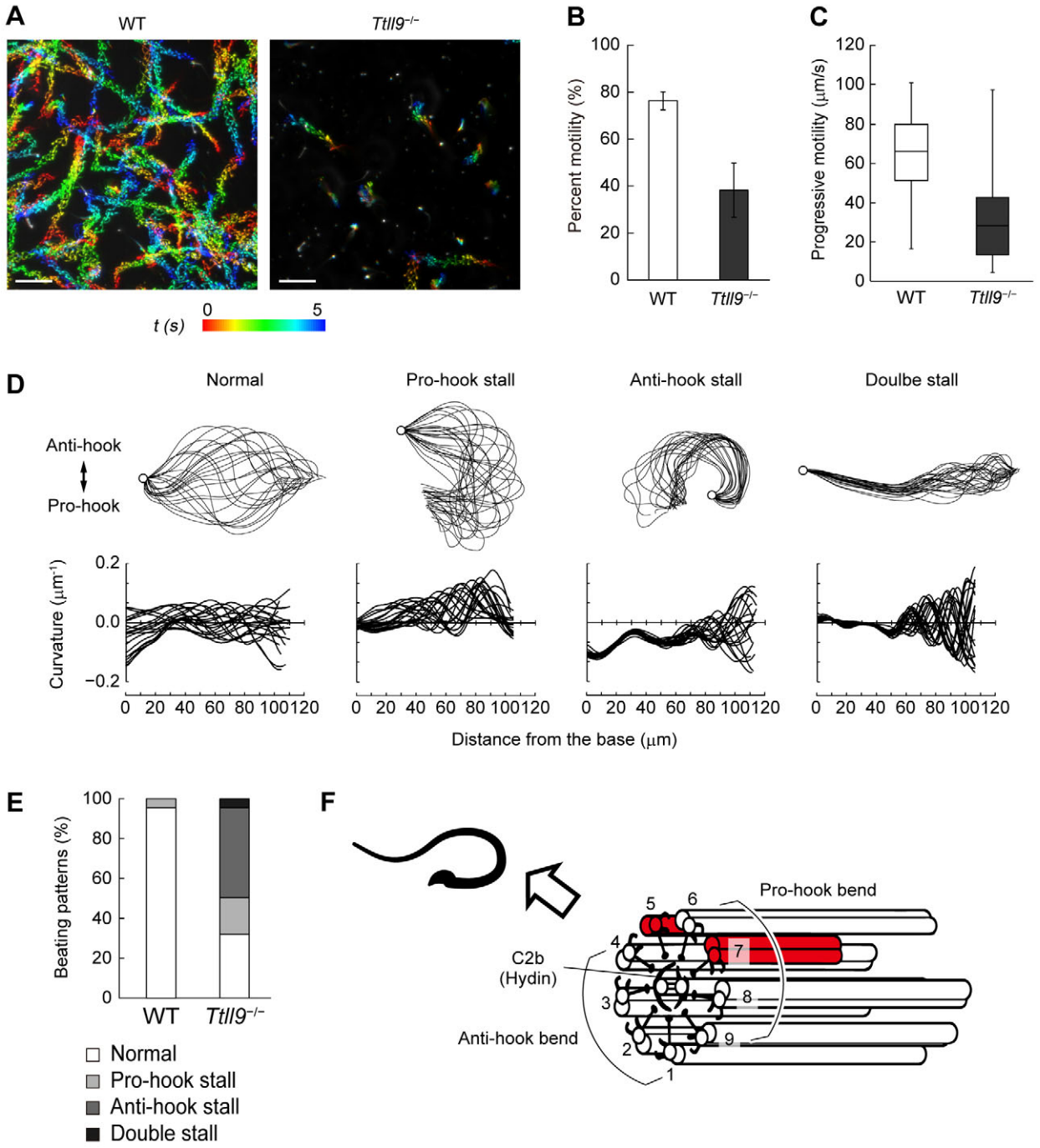

Fig. 4. Sperm motility analyses. (A) Trajectories of wild-type (WT) and *Ttll9*$^{-/-}$ spermatozoa visualized with superposed time-lapse images at 0.1-ms intervals for 5 s. The changing colors represent the time course from *t*=0 s (red) to 5 s (blue). Scale bars: 100 µm. (B) Percent motility of spermatozoa. *n*=786 (WT) and 713 (*Ttll9*$^{-/-}$). *P*=0.020 (Student's *t*-test, two-tailed). Data are mean±s.e.m. (C) Progressive motility of spermatozoa. *n*=104 (WT) and 90 (*Ttll9*$^{-/-}$). *P*<0.001 (Student's *t*-test, two-tailed). Lines represent the medians, boxes represent quartiles, and whiskers represent maximum and minimum values. (D) Representative superpositions of normal and three stall waveforms for 0.5-s at 20-ms intervals (top), and corresponding curvature plots (bottom). For top panels, empty circles indicate the position of flagellar bases. (E) Percentage of flagella showing the beat patterns detailed in D. *n*=21 (WT) and *n*=22 (*Ttll9*$^{-/-}$). (F) Schematic drawing of the geometry of axonemal components in flagella of murine spermatozoa. The most affected doublets in *Ttll9*$^{-/-}$ flagella are highlighted (red). Doublet 5 is located close to hydin (C2b), which is important for switching of flagellar beating. Doublet 7 was also found to be shortened. One or both of the defects in the two doublets could underlie the frequent anti-hook stall of *Ttll9*$^{-/-}$ flagella. *n* values represent the number of spermatozoa analyzed.

major group of proteins to be abundantly polyglutamylated in spermatozoa (Fig. S1E). Tubulins bind to VDACs through their negatively charged CTTs (Rostovtseva et al., 2008). Therefore, reduced polyglutamylation is expected to weaken the interaction between VDACs and tubulins, which might be the cause of similar structural phenotypes between *Vdac3* and *Ttll9* mutants. Future research on the exact localization of VDACs and their interactions with tubulins in flagella would provide useful information to reveal the molecular mechanisms underlying selective loss of doublet 7 in V*dac*3- and *Ttll9*-deficient mice.

Journal of Cell Science (2016) 129, 2757-2766 doi:10.1242/jcs.185983

The other heterogeneous effect of the loss of TTLL9 on outer doublet MTs is the greatest reduction of polyglutamylation in doublet 5, suggesting some selectivity of TTLL9. Doublet 5 of sea urchin sperm flagella and a corresponding doublet of *Chlamydomonas* flagella (doublet 1) have been reported to be structurally different from other doublets (Lin et al., 2012). This structural uniqueness of doublet 5 is likely to be conserved in murine sperm flagella (Lindemann et al., 1992). The structural heterogeneity might allow preferential, if not exclusive, recruitment of TTLL9 to doublet 5. This also indicates the possibility of other TTLLs that have selectivity for a specific doublet. Structural heterogeneity is not limited to doublet 5. For example, I1 inner arm dyneins on doublets 3 and 4 are structurally different from those of other doublets in *Chlamydomonas* flagella (Heuser et al., 2012). It is tempting to speculate that structural heterogeneity can affect the affinity of tubulin-modifying enzymes to specific MT subsets in sperm axonemes. The idea of 'division of labor' among TTLLs is also supported by the fact that *Stamp*$^{tm/tm}$ mice show specific loss of doublet 4 in sperm flagella (Lee et al., 2013). No obvious ciliary phenotypes in other tissues suggest that TTLL9 has, if any, only a minor function, or that its function is compensated by other TTLLs there. It will be interesting to investigate whether other TTLLs have a similar role in other cell types in future.

The polyglutamylation levels in the testes, whole sperm and proximal part of sperm flagella of *Ttll9*$^{-/-}$ mice were 50–70% of those in wild type. The polyglutamylation level on doublet 5 in *Ttll9*$^{-/-}$ mice was also ∼60% of that in wild type. An argument that such a reduction could have an impact on flagellar structure and motility is possible. A unique property of polyglutamylation is that even its moderate reduction can cause remarkable effects on the microtubular system – e.g. motility defects of the cilia in *Tetrahymena* (Suryavanshi et al., 2010). Therefore, it is not surprising that the partial reduction of polyglutamylation caused by *Ttll9* loss can have significant effects on axonemal structures and motility. It is also important to note that the severe reduction of the PTM inhibits normal flagellogenesis of mouse spermatozoa (Ikegami et al., 2010). Therefore, 'hypomorphic' mutants of polyglutamylation, like *Ttll9*$^{-/-}$ mice, offer a valuable opportunity to study polyglutamylation in mammalian sperm flagella.

Ttll9 deficiency strongly affected the beating pattern of murine sperm flagella, in contrast with the *Chlamydomonas* mutant lacking functional TTLL9, which shows an almost normal beating pattern (Kubo et al., 2010, 2012). We often observed active beats of *Ttll9*$^{-/-}$ spermatozoa at distal flagellum that showed a stall at the proximal region (Movie 2). This seems to contradict the observation that doublet 7 is frequently missing at distal flagellum. Because *Stamp*$^{tm/tm}$ spermatozoa that lack doublet 4 are reportedly motile (Lee et al., 2013), one possible explanation for the motile distal flagellum in *Ttll9*$^{-/-}$ spermatozoa is that the loss of a single doublet can be compensated by other doublets. However, a more convincing explanation is that the motile distal flagellum retains all doublets because about half of flagella should still have nine doublets, even at the end piece (Fig. 3E). Longitudinal heterogeneity of polyglutamylation might also be associated with stalls at proximal flagella. In murine spermatozoa, the polyglutamylation level is highest at the flagellar base and decreases toward the tip (Fouquet et al., 1996). Therefore, the effect of reduced polyglutamylation must be more severe at proximal flagella.

Several studies have reported the importance of tubulin polyglutamylation in ciliary and flagellar motility. Coordinated activation of axonemal dyneins and cyclic interdoublet sliding are essential for smooth bending propagation along flagella and cilia (Satir, 1985). Because reduced polyglutamylation alters the dynein–MT interaction (Suryavanshi et al., 2010; Kubo et al., 2010; Sirajuddin et al., 2014; Alper et al., 2014), reduced polyglutamylation in *Ttll9*$^{-/-}$ axonemes is likely to be the cause of stalls. According to one of the promising models for flagellar motility, the geometric clutch model, mechanical stress imposed on doublets plays a key role for normal beating (Lindemann and Lesich, 2010, 2015). The model assumes that flagellar bending generates forces that are transverse to the outer doublets (t-forces), which would pry interacting doublet pairs apart to cease sliding. Kubo et al. (2010) suggest that the reduced polyglutamylation could weaken the interaction between the C-terminal tails of tubulins and the positively charged stalk tips of dyneins. The weakened affinity should alter the threshold of the geometric clutch mechanism and might cause the frequent stalls.

Frequent anti-hook stalls observed in *Ttll9*$^{-/-}$ sperm flagella seem to be caused by the failure of bend switching after the anti-hook bend. This can be explained, at least partly, by the geometry of the axoneme in murine spermatozoa. Doublet 1 is located at the hook side of the head, and doublets 5 and 6 are at the anti-hook side in murine sperm flagella (Fig. S2K). Dynein arms protrude clockwise, when seen from the base (Gibbons, 1963). According to the ultrastructural geometry and the switch point hypothesis of ciliary beating (Satir and Matusoka, 1989), the pro-hook bend is directed towards doublets 5 and 6 through the activity of dyneins on doublets 6–9, and the anti-hook bend is directed towards doublet 1 through the activity of dyneins on doublets 1–4 (Fig. 4F). A possible explanation is a defect in switching signals from the central apparatus to doublet 5. Supporting this scenario, interestingly, mice with a defective central apparatus protein, hydin, show frequent stalls of ependymal cilia (Lechtreck et al., 2008), which is similar to what is observed in *Ttll9*$^{-/-}$ sperm flagella. Because the C2b projection on the central apparatus is missing in the hydin-deficient cilia, the C2b projection is thought to be essential for switching of bending directions. Because the central pair in Metazoa does not rotate, the C2b projection is always located close to, and has possible interactions with, doublets 4 and 5 (Fig. 4F), where the most severe effect of *Ttll9*$^{-/-}$ loss is expected. Although the C2b projection is present in *Ttll9*$^{-/-}$ flagella, defects in the function or mechanical property of doublet 5 downstream of C2b signaling likely mimic some features of C2b loss, that is, frequent stalling in *Ttll9*$^{-/-}$ flagella. An alternative explanation is the failure of pro-hook bend initiation as a result of a defective doublet 7. Because doublet 7 is one of nine doublets that is expected to work during pro-hook bending (Fig. 4F), its deficiency could impair the initiation of pro-hook bend. A shortened doublet 7 would perturb any feedback system from distal to proximal flagellum (Hayashi and Shingyoji, 2008).

Our data suggest that TTLL9 is involved in the establishment of heterogeneity among doublet MTs, which is essential for structural and functional integrity of murine sperm flagella. Although structural and biochemical heterogeneity among individual doublets has not been highlighted in modelling ciliary and flagellar beating (Lindemann and Lesich, 2010), our results emphasize the importance of interdoublet heterogeneities in normal axonemal structures and functions. Interestingly, the phenotype of *Ttll9*$^{-/-}$ sperm flagella is quite different from that observed in the flagella of *Ttll9*-deficient *Chlamydomonas*, where no severe structural and motility defects are seen. The inconsistency seems to reflect the differences in polyglutamylation patterns, accessory structures and mechanisms to regulate axonemal motility, highlighting the importance of comparative studies on various cilia and flagella.

Journal of Cell Science (2016) 129, 2757-2766 doi:10.1242/jcs.185983

MATERIALS AND METHODS

Animals

Wild-type (WT) mice of the C57BL/6N strain were purchased for breeding from CLEA Japan (Tokyo, Japan). All experiments were performed in accordance with guidelines issued by the Institutional Animal Care and Use Committees of Hamamatsu University, School of Medicine.

For *Ttll9* gene disruption, exons 4–5 were replaced with a *neo* cassette by homologous recombination in RENKA embryonic stem cells in the C57BL/6N background (Mishina and Sakimura, 2007). PCR-based genotyping was performed on genomic DNA extracted from mouse tails. The following primers were used: *Ttll9*$^{-/-}$ primer, 5′-GACGTGCTACTTCCATTTGTC-3′; wild-type primer, 5′-CTCTAGAGAGCTCCAACACTT-3′; and common primer, 5′-GCACCTTAGGAAGTAGTTGAG-3′. Expected PCR products were 547 bp for the wild-type allele and 443 bp for the *Ttll9*$^{-/-}$ allele. For *in vivo* fertilization assays, *Ttll9*$^{-/-}$ and wild-type males at 8–9 weeks of age were mated one-to-one with 8-week-old C57BL/6N females for a period of no longer than 2 months.

RT-PCR

Total RNA was extracted with Sepasol-RNA I Super (Nacalai Tesque, Kyoto, Japan) from various tissues and reverse-transcribed with ReverTra Ace (Toyobo, Osaka, Japan). The following primers were used to examine the expression of *Ttll9*: full-length *Ttll9* (accession number NM_001083618), forward (*Ttll9*-F) 5′-ATGTCGCGACAGAAGAATC-3′, reverse (*Ttll9*-R) 5′-TCAGCTAGGGGCTTTCC-3′; as an internal control *Gapdh* (accession number GU214026), forward 5′-TGCCCCCATGTTTGTGATG-3′, reverse 5′-TGTGGTCATGAGCCCTTCC-3′. Wild-type and *Ttll9*$^{-/-}$ transcripts were examined with the following primers: exons 1–15, forward *Ttll9*-F, reverse *Ttll9*-R; exons 1–3, forward *Ttll9*-F, reverse 5′-TTTGACTTCCACCCATCC-3′; exons 4–5, forward 5′-GAAGGCGAATGGGATTTC-3′, reverse 5′-AGGCTTCATGATCCAGGTG-3′; exons 6–15, forward 5′-TCATGGACTGGAGGAAGG-3′, reverse *Ttll9*-R.

In situ hybridization

Wild-type mouse testes were fixed in 4% paraformaldehyde and cryopreserved with sucrose in PBS. Testes were then embedded in optimal cutting temperature compound (SAKURA Finetek, Tokyo, Japan) and sliced into 20-µm-thick sections. Full-length *Ttll9* was inserted into the TOPO vector (Life Technologies) and linearized for the synthesis of a DIG-labeled probe. *In vitro* transcription and *in situ* hybridization were performed as previously described (Mukai et al., 2009).

Hematoxylin and eosin staining

Testes excised from 8-week-old *Ttll9*$^{-/-}$ mice and wild-type mice were snap-frozen in powdered dry ice and sliced into 10-µm-thick sections with a cryostat (CM1950 Cryostat, Leica Microsystems, Wetzlar, Germany). The histological sections were stained with Mayer's hematoxylin and eosin (Sakura Finetek). Histological images were obtained with a Leica LMD6000 laser microdissection microscope (Leica Microsystems) with a 10× objective lens (Leica HCX PL FLUOTAR 10×/0.30) and Hitachi HV-D20 CCD camera (Hitachi Kokusai Electric, Tokyo, Japan) and Leica Laser Microdissection software v6.5 (Leica Microsystems).

Epididymal sperm count

The number of spermatozoa in the cauda epididymides of 8-week-old mice was counted based on an established method (Wang, 2003). Briefly, cauda epididymides were weighed and minced in 2 ml of PBS. After a 15-min incubation at 37°C, a homogeneous sperm suspension was obtained after pipetting up and down. The sperm suspension was then diluted with PBS, and the spermatozoa were immobilized by heating at 60°C for 1–2 min. The number of spermatozoa was estimated by loading 10 µl of sperm suspension onto a Neubauer hemocytometer, and normalized using the weight of the cauda epididymides.

SDS-PAGE and western blotting

A pair of cauda epididymis from a single mouse were minced in 2 ml of PBS and incubated for 15 min at 37°C. The sperm suspension was centrifuged, and the sperm pellet was retrieved and washed twice with PBS. SDS-PAGE sample buffer was added to the sperm pellet, the mixture was sonicated, and the supernatant was collected after centrifugation at 200,000 ***g*** for 10 min at 4°C. Proteins were separated in 10% acrylamide gel and then transferred onto a PVDF membrane. PVDF membranes were first treated with blocking solution 1 (7.5% skimmed milk, 0.1% Tween-20 in TBS) at room temperature for 1 h and then incubated with anti-polyglutamate side-chain antibody (polyE, 1:3000), anti-α-tubulin antibody (12G10; 1:2000; Developmental Studies Hybridoma Bank), or anti-VDAC3 antibody (1:1000; Proteintech) in blocking solution 1 for 1 h. After several washes with 0.1% Tween-20 in TBS, the membrane was incubated for 1 h with goat anti-rabbit-IgG antibody horseradish peroxidase (HRP) conjugate (1:10,000; Jackson ImmunoResearch Laboratory) for polyE and anti-VDAC3 antibodies, or goat anti-mouse-IgG antibody HRP conjugate (1:10,000, Jackson ImmunoResearch Laboratory). The membrane was then washed several times with 0.1% Tween-20 in TBS and treated with Amersham ECL western blotting detection reagents (GE Healthcare, Little Chalfont, UK). Chemiluminescence was detected with a luminescent image analyzer, LAS-3000 mini (Fujifilm, Tokyo, Japan). For quantitative analysis, whole testis or sperm proteins from three wild-type and three *Ttll9*$^{-/-}$ individuals were blotted on the same membrane to ensure the same conditions during immunostaining. Signal intensity of the original 16-bit TIFF images was quantified with ImageJ software (National Institute of Health).

Transmission electron microscopy

Testes or cauda epididymides were fixed with 2% glutaraldehyde in 0.067 M phosphate buffer (pH 7.4) for 2 h at 4°C. After several washes with phosphate buffer, they were post-fixed with 1% osmium tetroxide in 0.067 M phosphate buffer for 2 h, dehydrated with an ascending series of ethanol and propylene oxide, and embedded in Quetol-812 (Nisshin EM Corporation, Tokyo, Japan). Ultrathin sections of 80–100 nm in thickness were cut with an ultramicrotome (Ultracut UCT, Leica Mycrosystems). Following consecutive staining with uranyl acetate for 5 min and lead stain solution (Sigma-Aldrich) for 3 min, carbon was deposited with the JEOL JEE-4X vacuum evaporator (JEOL, Tokyo, Japan). The sections were observed with a JEOL 1220 electron microscope (JEOL) at 80 kV. Electron micrographs were taken with Bioscan Camera Model 792 and DigitalMicrograph software (Gatan, CA, USA).

Immunoelectron microscopy

A previously described method was modified and used for immunoelectron microscopy (Kann and Fouquet, 1989). Cauda epididymides were fixed with 1% glutaraldehyde and 0.1 M phosphate buffer (pH 7.4) for 2 h at 4°C. After several washes with 0.1 M phosphate buffer, cauda epididymides were dehydrated with a series of ethanol solutions. The specimen was then moved into LR White and solidified by heating at 55°C for 24 h. The blocks were sliced into 80- to100-nm thick sections, and the sections were attached to nickel grids. These sections were treated with blocking solution 2 (150 mM NaCl, 0.1% BSA, 10 mM glycine in 20 mM Tris-HCl, pH 7.8) for 1 h, rinsed with TBS and treated with primary antibody DM1A (1:1000) or polyE (1:1000) diluted with blocking solution 2 for 1 h. After several rinses with TBS, sections on the nickel grids were treated with goat anti-mouse-IgG 10-nm gold for DM1A (1:50) or goat anti-rabbit-IgG 10-nm gold for polyE (1:50) (BBI solutions, Cardiff, UK) for 1 h. Sections on the nickel grids were then rinsed with TBS and distilled water several times, and stained with uranyl acetate for 30 s and lead stain solution for 10 s. Carbon deposition and analysis of the sections were conducted as described above for TEM. For quantitative analysis of the heterogeneous polyglutamylation patterns, the number of the gold particles on ultrathin sections of cauda epididymides from wild-type and a *Ttll9*$^{-/-}$ mice were counted. The results of three experiments with independent sperm samples were standardized, and mean values were acquired from the three experiments.

Sperm motility analyses

Cauda epididymides were excised from *Ttll9*$^{-/-}$ and wild-type mice, minced in modified Tyrode's albumin lactate pyruvate (mTALP) medium, which had been pre-equilibrated under 5% CO_2 at 37°C for at least 1 h. The fragments of cauda epididymis were incubated in a CO_2 incubator for 10 min to allow

sperm to swim out. The medium with spermatozoa was suspended, loaded onto a Leja® Standard Count 2 Chamber Slide (#SC 20-01-02-B, Leja, Nieuw-Vennep, The Netherlands) and recorded at room temperature at 200 or 500 frame per second (fps) with a digital high-speed camera HAS-L1 (DITECT, Tokyo, Japan) attached to an Eclipse TE2000-U (Nikon, Tokyo, Japan) or Leica DMI3000B (Leica Microsystems) microscope. The objective lenses used were either Plan Fluor 4×/0.13 and Plan Fluor 10×/030 on Eclipse TE2000-U or N PLAN 5×/0.12 and HC PL APO 10×/0.40 on Leica DMI3000B. For trajectory superposition, sequential images at 200 fps obtained as above were downsized to 10 fps. Images for 5 s at 10 fps (50 images in total) were superposed with ImageJ software with Color FootPrint (http://www.jaist.ac.jp/ms/labs/hiratsuka/images/0/09/Color_FootPrint.txt) to show sperm swimming trajectories as a spectrum of colors.

For curvature analysis, original images were downsized to 50 fps using ImageJ. Only spermatozoa showing no rotation for at least more than 0.5 s were selected. Cell motility analysis software, Bohboh (Bohbohsoft, Tokyo, Japan), was used to trace flagella and calculate their curvatures (Baba and Mogami, 1985). Flagella of the selected spermatozoa were traced automatically in each frame. Traces were visually checked and manually corrected when needed. To superpose flagellar traces, the flagellar base was considered the reference point, and the imaginary line between the flagellar base and tip was used as the reference line (see also Fig. S3A). After flagellar traces were arranged as described above, curvatures along a flagellum were calculated and plotted as a function of the distance from the base of the flagellum. Flagellar curvature was defined as the inverse of the radius of the osculating circle at a given point on a flagellum. Curvature plots for 0.5 s at every 20 ms were considered superpositions of the flagellar traces (Fig. S3B,C). Beat direction was determined by the hook-shaped heads of the spermatozoa by adopting the principles of Ishijima et al. (2002) – the pro-hook bend follows the direction that the hook is pointing, and the anti-hook bend was opposite to that of the pro-hook bend. To distinguish between pro- and anti-hook bends, the anti-hook bend curvature was represented as a negative value (Fig. S3B,C). We classified beating patterns into four classes from the viewpoint of stall patterns: (1) normal beat, curvature at any point on a flagellum takes both positive and negative values; (2) pro-hook stall, a given point on a flagellum maintains a pro-hook bend state (only positive value in the curvature within a 0.5 s time frame); (3) anti-hook stall, the opposite of pro-hook stall (only negative values in the curvature); (4) double stall, pro-hook and anti-hook stalls occur at the same time on a single flagellum.

Image processing

Brightness and contrast of the images presented here were adjusted with Adobe PhotoShop Elements 12 (Adobe Systems). Charts were made with Excel® 2013 (Microsoft) and modified with Adobe Illustrator CS6 (Adobe Systems) to maintain the original values and proportions. Movie Maker® (Microsoft) was used to edit the movie files.

Acknowledgements

We thank members of our laboratory for critical reading of the manuscript. We also grateful for Showbu Sato, Kenji Nakamura, Mineo Matsumoto, Reiko Tsuchiya and Shouko Takamatsu at the Mitsubishi Kagaku Institute of Life Sciences for technical support. The monoclonal antibody 12G10, originally developed by J. Frankel and E. M. Nelsen was obtained from the Developmental Studies Hybridoma Bank, created by the National Institute of Child Health and Human Development of the National Institutes of Health and maintained at the Department of Biology, University of Iowa, Iowa City, IA

Competing interests

The authors declare no competing or financial interests.

Author contributions

A.K., K. Ikegami, Y.K. and M.S. conceived the research. A.K., K. Ikegami and Y.K. designed experiments. A.K. performed almost all experiments and data analyses. H.-J.Y., M.A, M.Y. and K.S. generated *Ttll9*$^{-/-}$ mice. K.S. and K. Inaba provided software to analyze flagellar motility and wave form, and supported sperm motility analyses. A.K., K. Ikegami, I.Y. and M.S. wrote the manuscript.

Funding

This work was supported by Japan Society for the Promotion of Science KAKENHI [grant numbers 12J06986 (to A.K.) and 15H01316 (to K.I.)].

Supplementary information

Supplementary information available online at
http://jcs.biologists.org/lookup/doi/10.1242/jcs.185983.supplemental

References

Alper, J. D., Decker, F., Agana, B. and Howard, J. (2014). The motility of axonemal dynein is regulated by the tubulin code. *Biophys. J.* **107**, 2872-2880.

Baba, S. A. and Mogami, Y. (1985). An approach to digital image analysis of bending shapes of eukaryotic flagella and cilia. *Cell Motil.* **5**, 475-489.

Bosch Grau, M., Gonzalez Curto, G., Rocha, C., Magiera, M. M., Marques Sousa, P., Giordano, T., Spassky, N. and Janke, C. (2013). Tubulin glycylases and glutamylases have distinct functions in stabilization and motility of ependymal cilia. *J. Cell Biol.* **202**, 441-451.

Eddé, B., Rossier, J., Le Caer, J. P., Desbruyères, E., Gros, F. and Denoulet, P. (1990). Posttranslational glutamylation of α-tubulin. *Science* **247**, 83-85.

Fouquet, J.-P., Prigent, Y. and Kann, M.-L. (1996). Comparative immunogold analysis of tubulin isoforms in the mouse sperm flagellum: unique distribution of glutamylated tubulin. *Mol. Reprod. Dev.* **43**, 358-365.

Gibbons, I. R. (1963). A method for obtaining serial sections of known orientation from single spermatozoa. *J. Cell Biol.* **16**, 626-629.

Hayashi, S. and Shingyoji, C. (2008). Mechanism of flagellar oscillation-bending-induced switching of dynein activity in elastase-treated axonemes of sea urchin sperm. *J. Cell Sci.* **121**, 2833-2843.

Heuser, T., Barber, C. F., Lin, J., Krell, J., Rebesco, M., Porter, M. E. and Nicastro, D. (2012). Cryoelectron tomography reveals doublet-specific structures and unique interactions in the I1 dynein. *Proc. Natl. Acad. Sci. USA* **109**, E2067-E2076.

Hinsch, K.-D., De Pinto, V., Aires, V. A., Schneider, X., Messina, A. and Hinsch, E. (2004). Voltage-dependent anion-selective channels VDAC2 and VDAC3 are abundant proteins in bovine outer dense fibers, a cytoskeletal component of the sperm flagellum. *J. Biol. Chem.* **279**, 15281-15288.

Ikegami, K., Mukai, M., Tsuchida, J.-i., Heier, R. L., Macgregor, G. R. and Setou, M. (2006). TTLL7 is a mammalian β-tubulin polyglutamylase required for growth of MAP2-positive neurites. *J. Biol. Chem.* **281**, 30707-30716.

Ikegami, K., Sato, S., Nakamura, K., Ostrowski, L. E. and Setou, M. (2010). Tubulin polyglutamylation is essential for airway ciliary function through the regulation of beating asymmetry. *Proc. Natl. Acad. Sci. USA* **107**, 10490-10495.

Inaba, K. (2007). Molecular basis of sperm flagellar axonemes: structural and evolutionary aspects. *Ann. N. Y. Acad. Sci.* **1101**, 506-526.

Inaba, K. (2011). Sperm flagella: comparative and phylogenetic perspectives of protein components. *Mol. Hum. Reprod.* **17**, 524-538.

Ishijima, S., Baba, S. A., Mohri, H. and Suarez, S. S. (2002). Quantitative analysis of flagellar movement in hyperactivated and acrosome-reacted golden hamster spermatozoa. *Mol. Reprod. Dev.* **61**, 376-384.

Janke, C., Rogowski, K., Wloga, D., Regnard, C., Kajava, A. V., Strub, J.-M., Temurak, N., van Dijk, J., Boucher, D., van Dorsselaer, A. et al. (2005). Tubulin polyglutamylase enzymes are members of the TTL domain protein family. *Science* **308**, 1758-1762.

Kann, M.-L. and Fouquet, J.-P. (1989). Comparison of LR white resin, Lowicryl K4M and Epon postembedding procedures for immunogold staining of actin in the testis. *Histochemistry* **91**, 221-226.

Kann, M.-L., Soues, S., Levilliers, N. and Fouquet, J.-P. (2003). Glutamylated tubulin: diversity of expression and distribution of isoforms. *Cell Motil. Cytoskeleton* **55**, 14-25.

Konno, A., Setou, M. and Ikegami, K. (2012). Ciliary and flagellar structure and function—their regulations by posttranslational modifications of axonemal tubulin. *Int. Rev. Cell Mol. Biol.* **294**, 133-170.

Kubo, T., Yanagisawa, H.-a., Yagi, T., Hirono, M. and Kamiya, R. (2010). Tubulin polyglutamylation regulates axonemal motility by modulating activities of inner-arm dyneins. *Curr. Biol.* **20**, 441-445.

Kubo, T., Yagi, T. and Kamiya, R. (2012). Tubulin polyglutamylation regulates flagellar motility by controlling a specific inner-arm dynein that interacts with the dynein regulatory complex. *Cytoskeleton (Hoboken)* **69**, 1059-1068.

Kubo, T., Hirono, M., Aikawa, T., Kamiya, R. and Witman, G. B. (2015). Reduced tubulin polyglutamylation suppresses flagellar shortness in Chlamydomonas. *Mol. Biol. Cell* **26**, 2810-2822.

Lechtreck, K.-F., Delmotte, P., Robinson, M. L., Sanderson, M. J. and Witman, G. B. (2008). Mutations in Hydin impair ciliary motility in mice. *J. Cell Biol.* **180**, 633-643.

Lee, J. E., Silhavy, J. L., Zaki, M. S., Schroth, J., Bielas, S. L., Marsh, S. E., Olvera, J., Brancati, F., Iannicelli, M., Ikegami, K. et al. (2012). CEP41 is mutated in Joubert syndrome and is required for tubulin glutamylation at the cilium. *Nat. Genet.* **44**, 193-199.

Lee, G.-S., He, Y., Dougherty, E. J., Jimenez-Movilla, M., Avella, M., Grullon, S., Sharlin, D. S., Guo, C., Blackford, J. A., Jr., Awasthi, S. et al. (2013). Disruption of Ttll5/stamp gene (tubulin tyrosine ligase-like protein 5/SRC-1 and TIF2-associated modulatory protein gene) in male mice causes sperm malformation and infertility. *J. Biol. Chem.* **288**, 15167-15180.

Lin, J., Heuser, T., Song, K., Fu, X. and Nicastro, D. (2012). One of the nine doublet microtubules of eukaryotic flagella exhibits unique and partially conserved structures. *PLoS ONE* **7**, e46494.
Lindemann, C. B. and Lesich, K. A. (2010). Flagellar and ciliary beating: the proven and the possible. *J. Cell Sci.* **123**, 519-528.
Lindemann, C. B. and Lesich, K. A. (2015). The geometric clutch at 20: stripping gears or gaining traction? *Reproduction* **150**, R45-R53.
Lindemann, C. B., Orlando, A. and Kanous, K. S. (1992). The flagellar beat of rat sperm is organized by the interaction of two functionally distinct populations of dynein bridges with a stable central axonemal partition. *J. Cell Sci.* **102**, 249-260.
Liu, B., Wang, Z., Zhang, W. and Wang, X. (2009). Expression and localization of voltage-dependent anion channels (VDAC) in human spermatozoa. *Biochem. Biophys. Res. Commun.* **378**, 366-370.
Magiera, M. M. and Janke, C. (2014). Post-translational modifications of tubulin. *Curr. Biol.* **24**, R351-R354.
Mishina, M. and Sakimura, K. (2007). Conditional gene targeting on the pure C57BL/6 genetic background. *Neurosci. Res.* **58**, 105-112.
Mukai, M., Ikegami, K., Sugiura, Y., Takeshita, K., Nakagawa, A. and Setou, M. (2009). Recombinant mammalian tubulin polyglutamylase TTLL7 performs both initiation and elongation of polyglutamylation on β-tubulin through a random sequential pathway. *Biochemistry* **48**, 1084-1093.
Pathak, N., Austin, C. A. and Drummond, I. A. (2011). Tubulin tyrosine ligase-like genes ttll3 and ttll6 maintain zebrafish cilia structure and motility. *J. Biol. Chem.* **286**, 11685-11695.
Prigent, Y., Kann, M. L., Lach-Gar, H., Péchart, I. and Fouquet, J. P. (1996). Glutamylated tubulin as a marker of microtubule heterogeneity in the human sperm flagellum. *Mol. Hum. Reprod.* **2**, 573-581.
Rostovtseva, T. K., Sheldon, K. L., Hassanzadeh, E., Monge, C., Saks, V., Bezrukov, S. M. and Sackett, D. L. (2008). Tubulin binding blocks mitochondrial voltage-dependent anion channel and regulates respiration. *Proc. Natl. Acad. Sci. USA* **105**, 18746-18751.
Sampson, M. J., Decker, W. K., Beaudet, A. L., Ruitenbeek, W., Armstrong, D., Hicks, M. J. and Craigen, W. J. (2001). Immotile sperm and infertility in mice lacking mitochondrial voltage-dependent anion channel type 3. *J. Biol. Chem.* **276**, 39206-39212.
Satir, P. (1985). Switching mechanisms in the control of ciliary motility. *Mod. Cell Biol.* **4**, 1-46.
Satir, P. and Matsuoka, T. (1989). Splitting the ciliary axoneme: implications for a "switch-point" model of dynein arm activity in ciliary motion. *Cell Motil. Cytoskeleton* **14**, 345-358.
Sirajuddin, M., Rice, L. M. and Vale, R. D. (2014). Regulation of microtubule motors by tubulin isotypes and post-translational modifications. *Nat. Cell Biol.* **16**, 335-344.
Suryavanshi, S., Eddé, B., Fox, L. A., Guerrero, S., Hard, R., Hennessey, T., Kabi, A., Malison, D., Pennock, D., Sale, W. S. et al. (2010). Tubulin glutamylation regulates ciliary motility by altering inner dynein arm activity. *Curr. Biol.* **20**, 435-440.
van Dijk, J., Rogowski, K., Miro, J., Lacroix, B., Eddé, B. and Janke, C. (2007). A targeted multienzyme mechanism for selective microtubule polyglutamylation. *Mol. Cell* **26**, 437-448.
van Dijk, J., Miro, J., Strub, J.-M., Lacroix, B., van Dorsselaer, A., Edde, B. and Janke, C. (2008). Polyglutamylation is a post-translational modification with a broad range of substrates. *J. Biol. Chem.* **283**, 3915-3922.
Wang, Y. (2003). Epididymal sperm count. *Curr. Protoc. Toxicol.* Chapter 16, Unit16.6.
Wloga, D. and Gaertig, J. (2010). Post-translational modifications of microtubules. *J. Cell Sci.* **123**, 3447-3455.
Wloga, D., Dave, D., Meagley, J., Rogowski, K., Jerka-Dziadosz, M. and Gaertig, J. (2010). Hyperglutamylation of tubulin can either stabilize or destabilize microtubules in the same cell. *Eukaryot. Cell* **9**, 184-193.
Zeisel, A., Muñoz-Manchado, A. B., Codeluppi, S., Lönnerberg, P., La Manno, G., Juréus, A., Marques, S., Munguba, H., He, L., Betsholtz, C. et al. (2015). Cell types in the mouse cortex and hippocampus revealed by single-cell RNA-seq. *Science* **347**, 1138-1142.